Fusion of Li and C and a search for entrance channel limitations to fusion cross sections

L. C. Dennis, K. M. Abdo,* A. D. Frawley, and K. W. Kemper
Department of Physics, Florida State University, Tallahassee, Florida 32306
(Received 22 February 1982)

Excitation functions have been measured for reaction products from the ^{6}Li and ^{7}Li induced reactions ^{6}Li+^{12}C, ^{6}Li+^{13}C, ^{7}Li+^{12}C, and ^{7}Li+^{13}C. These data cover the energy range from $E_{lab}=9$ to 36 MeV. It was found that the maximum fusion cross sections for these reactions are 780 and 770 mb for the ^{6}Li+^{12}C and ^{6}Li+^{13}C, respectively, and 960 and 930 mb for the ^{7}Li+^{12}C and ^{7}Li+^{13}C, respectively. The relative uncertainties for these maximum fusion cross sections are about 5%. Comparisons between optical model calculations of the total reaction cross sections and the measured fusion cross sections indicate that total fusion cross sections are substantially smaller than the total reaction cross sections for all four reactions at all energies. For each of the four entrance channels, energy and angular distributions have been measured at four energies for individual mass groups between $A=9$ and 19 u. Most of these products appear to be evaporation residues. The critical angular momenta deduced from the experimental fusion cross sections are discussed in terms of entrance channel and compound nucleus limitation models for compound nucleus formation. The individual mass groups are discussed in terms of systematics for evaporation residues.

[NUCLEAR REACTIONS ^{6}Li+^{12}C, $E_{^6\text{Li}}=10$ to 36 MeV; ^{6}Li+^{13}C, $E_{^6\text{Li}}=9.23$ to 35.08 MeV; ^{7}Li+^{12}C, $E_{^7\text{Li}}=10$ to 38 MeV; ^{7}Li+^{13}C, $E_{^7\text{Li}}=10$ to 34 MeV, measured $d^2\sigma/d\Omega\,dE$ for reaction products from $A=9$ to 19. Extracted σ_{fus}.]

I. INTRODUCTION

Considerable effort has been devoted to the study of total fusion cross sections as a function of bombarding energy. One of the more intriguing findings of such studies is the observation of a strong dependence of the maximum fusion cross section on the entrance channel.[1,2] Numerous models have been presented to try to explain the observed maximum fusion cross sections and the dependence of the fusion cross section on energy.[3–5] Complete understanding of the fusion process, however, awaits further studies. A study by Eck *et al.*[6] of the ^{9}Be + ^{28}Si fusion cross section revealed that the fusion cross section is significantly smaller than the total reaction cross section for this reaction, even at low bombarding energies. This experimental result might lead one to speculate that there is something unusual about fusion reactions induced by very light ions. Using ^{6}Li and ^{7}Li as projectiles is particularly attractive because the presence of the "extra" neutron in ^{7}Li could be expected to have a substantial effect on the reaction mechanisms which compete with fusion. In the present paper we describe measurements of the fusion cross sections for four closely related entrance channels ^{6}Li + ^{12}C, ^{6}Li + ^{13}C, ^{7}Li + ^{12}C, and ^{7}Li + ^{13}C. These entrance channels were chosen to allow us to search for projectile effects on the fusion excitation functions.

A potential difficulty which arises in all measurements of fusion cross sections is that of determining which reaction products are fusion-evaporation residues and which reaction products result from some other mechanism. We have measured cross sections for individual mass groups to assist in making this identification.

We present a description of the experimental procedure and results in Secs. II and III, respectively. Section IV compares the experimental results with various models for the fusion excitation functions and cross sections for individual mass groups. The conclusions are summarized in the last section.

II. EXPERIMENTAL PROCEDURE

The cross sections for production of nuclei of $A > 7$ by the $^6Li + ^{12}C$, $^6Li + ^{13}C$, $^7Li + ^{12}C$, and $^7Li + ^{13}C$ entrance channels were measured using ^6Li and ^7Li beams obtained from the Florida State University super FN tandem Van de Graaff accelerator. Targets were either natural ^{12}C targets ($\sim 80\ \mu g/cm^2$ thickness) or 97% enriched ^{13}C targets ($\sim 150\ \mu g/cm^2$ thickness). The heavy particles were identified by measuring flight times along a 2.7 m flight path. The start signal was obtained using a microchannel plate start detector. A 450 mm^2 silicon surface barrier detector was used to obtain the stop signal. The silicon surface barrier detector also gave the energy of each particle. The flight times and the energies of the residues provided mass identification of all particles for which $A > 7$. A typical two dimensional time-of-flight mass versus energy spectrum is shown in Fig. 1. The particles which we included in the fusion cross sections had masses of $A \geq 9$. The relatively small yields in the discrete peaks in the mass 9 group were not included. The efficiency of the time-of-flight system for any particle varies with the particle's mass and energy. The variation in efficiency is due to the changing number of electrons produced in the start detector. The efficiency of the time-of-flight system was found experimentally by comparing elastic scattering peaks in the singles surface barrier detector energy spectra to the corresponding peaks in the time-of-flight versus energy coincidence spectra for various beams and energies. In the energy range of interest the start detector was better than 97% efficient for particles with $A \geq 9$.

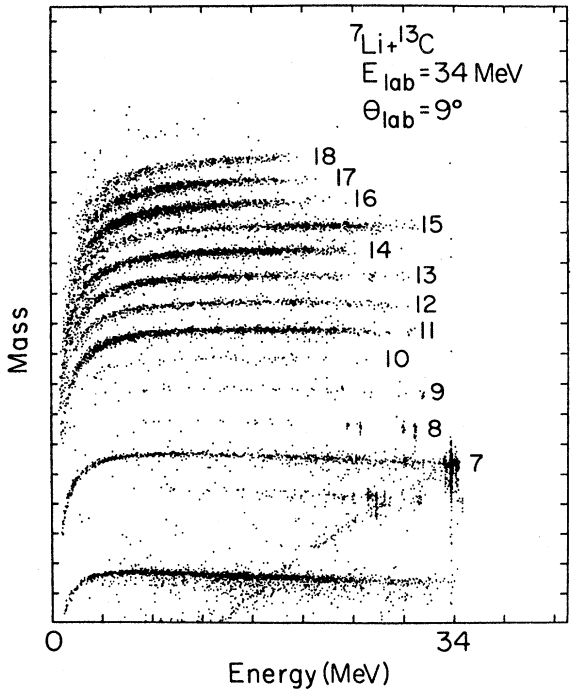

FIG. 1. Time-of-flight measurements for reaction products traversing a 2.7 m flight path yield the mass versus energy plot shown here. The time resolution was approximately 500 picoseconds.

The total cross sections for residues with $A > 7$ were obtained by integrating the angular distribution for each mass group at four selected energies. The measured angular distributions spanned the angular range from $\theta_{lab} = 5°$ to 45°; yields for angles outside this range were obtained by extrapolation. Table I details the energies and angles measured for each system. Selected angular distributions are shown in Fig. 2. In all cases the measured yields between the minimum and maximum angles account for at least 92% of the final reported integrated yields. The total cross sections at other energies were obtained by measuring the residue yields at one angle ($\theta_{lab} = 16°$ for the ^6Li induced reactions and $\theta_{lab} = 9°$ for the ^7Li induced reactions) and using the ratio of the single-angle yields to the total yields to interpolate smoothly between the four energies where the complete angular distributions were measured. This technique gives reliable excitation functions because the shapes of the angular distributions for the individual mass groups change slowly with energy.[7]

The absolute cross sections were obtained using two methods for each reaction. One method required obtaining absolute target thicknesses by measuring the yield for elastic scattering of 20 MeV ^{16}O at angles forward of 20° and assuming the scattering to be Rutherford. Absolute cross sections were also obtained by normalizing to the Li elastic scattering, which was found to be Rutherford when the beam energy was below 16 MeV and the detector angle was less than 10. The absolute cross sections obtained with these two methods agreed within 10% for each of the four reactions. The excitation functions obtained with the latter method are shown in Fig. 3. The relative uncertainties in the cross sections in one excitation function relative to those in another are approximately 5%.

Several checks were made on the relative cross sections for these four reactions. For example, the yield was measured for a ^6Li beam on a particular target at a single energy and over a small angular range. The beam was changed from ^6Li to ^7Li and the yields measured at the same angles on the same target spot. This procedure reduces the errors which arise in determining the relative cross sec-

TABLE I. Reactions, energies, and angles.

Reaction	Laboratory energy range (step size) (MeV)	Laboratory angles (deg)
$^{6}Li + ^{12}C$	10–36[2.0]	5, 7, 10, 13, 16, 19, 22, 25, 30, 35, 40, 45
$^{6}Li + ^{13}C$	9.23–35.08[1.85]	5, 7, 10, 13, 16, 19, 22, 25, 30, 35, 40, 45
$^{7}Li + ^{12}C$	10–38[2.0]	5, 7, 9, 11, 14, 17, 20, 24, 29, 34, 39, 44
$^{7}Li + ^{13}C$	10–34[2.0]	5, 7, 9, 11, 14, 17, 21, 25, 30, 35, 40, 45

tions due to target thickness variations. The resulting relative uncertainties for the excitation functions are 5% for different target and projectile combinations. These uncertainties are due to counting statistics, normalization of the excitation functions to the angular distributions, and uncertainties in sorting, integration, interpolation, and extrapolation procedures.

III. EXPERIMENTAL RESULTS

Shown in Figs. 4–7 are the total cross sections for the production of various mass groups as a function of the center of mass (c.m.) bombarding energy for the $^{6}Li + ^{12}C$, $^{6}Li + ^{13}C$, $^{7}Li + ^{12}C$, and $^{7}Li + ^{13}C$ entrance channels, respectively. The behavior of these excitation functions is roughly what one would expect from a fusion-evaporation reaction. Qualitatively we can explain the energy dependence of the mass groups in terms of the competition between the energetically allowed exit channels if we assume that sequential evaporation of protons, neutrons, and alpha particles dominates. Thus, for each reaction, the masses which can be produced by evaporating the same number of light particles from the compound nucleus peak at approximately the same center of mass energy. Furthermore, the mass groups corresponding to one, two, three, and four particle emission will peak at successively higher c.m. energies; each group will reach a maximum near the energy at which the next group begins to have a significant yield.

The evaporation of p, n, and α particles is expected, based on single step Hauser-Feshbach calculations, to comprise between 90 and 95% of the total evaporation yield for the first decay step. Thus sequential decays which include d, t, ^{3}He, ^{6}Li, or ^{8}Be evaporation at some step are expected to be relatively infrequent, but may not always be unimportant. One way in which the importance of other particle decays can be checked is by observing the maximum angle at which residues of a particular mass are detected and comparing this angle with the maximum angle allowed if the reaction proceeds via sequential emission of n, p, and α particles. In many cases the maximum kinematically allowed angle for sequential emission[2] is substantially lower than the maximum kinematically allowed angle for single particle emission. This difference arises because the Q values for the two-body final states are

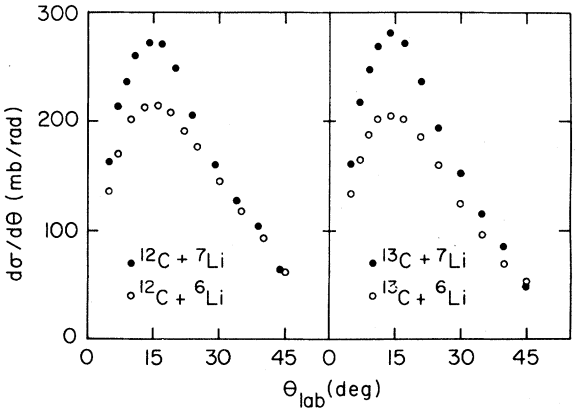

FIG. 2. Shown are some of the angular distributions which were integrated to determine the fusion cross section. The angular distributions are for the $^{12}C + ^{6}Li$, $^{12}C + ^{7}Li$, $^{13}C + ^{6}Li$, and $^{13}C + ^{7}Li$ reactions at E_{Li}=26, 30, 27.692, and 28 MeV, respectively.

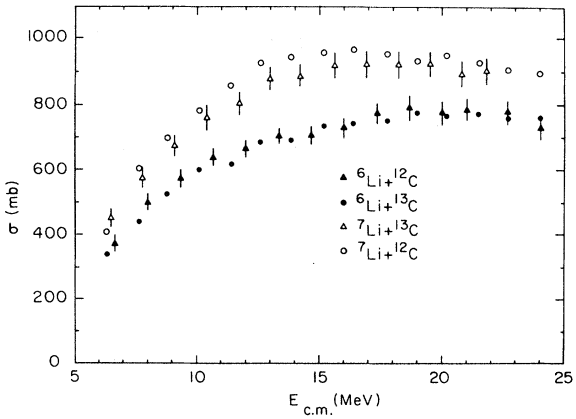

FIG. 3. The excitation functions for the total fusion cross sections are shown for all four reactions. The error bars give the relative errors appropriate for comparing the cross sections for the different reactions.

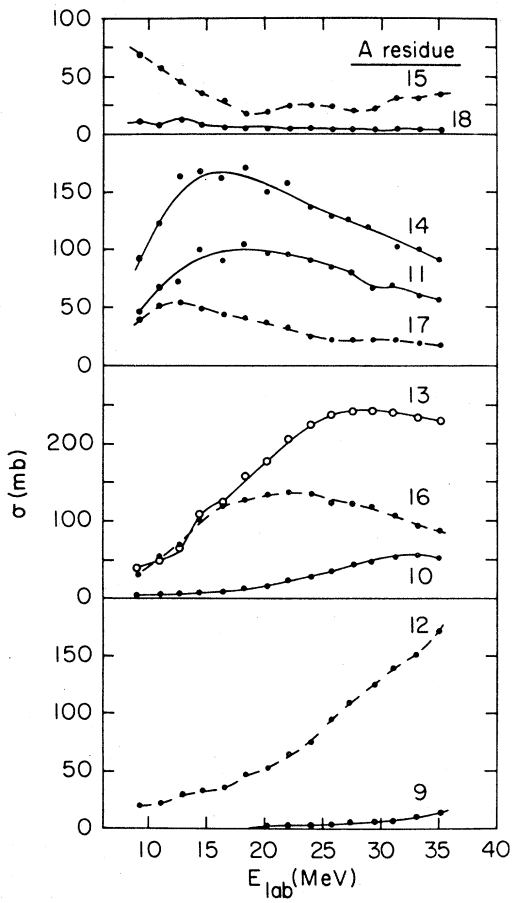

FIG. 4. Shown here are the excitation functions for the individual mass groups produced in the $^{6}Li + ^{12}C$ reaction. The lines are drawn to help guide the eye.

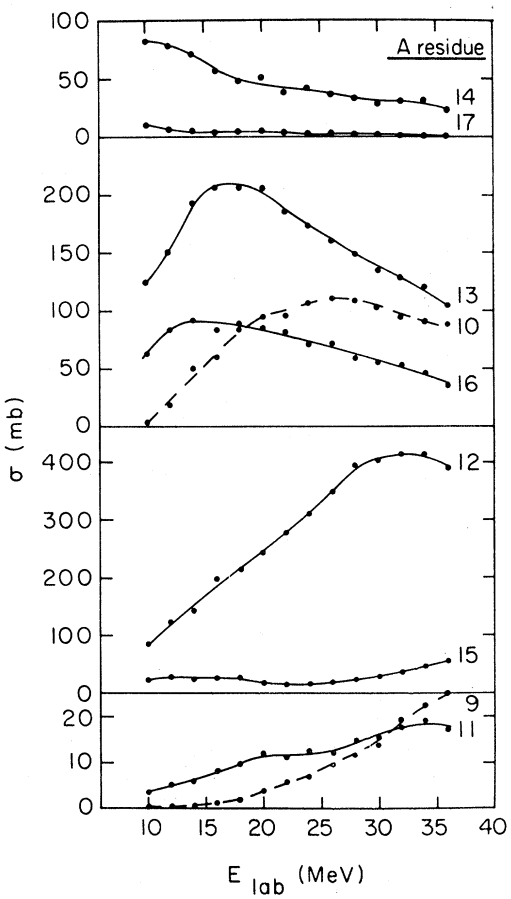

FIG. 5. Shown here are the excitation functions for the individual mass groups produced in the $^{6}Li + ^{12}C$ reaction. The lines are drawn to help guide the eye.

substantially larger than those for the three- or more-body final states. Shown in Table II are comparisons of the maximum angle predicted assuming sequential emission and the experimentally determined maximum angle for several mass groups of interest. As can be seen, differences in the maximum angles do exist for the residues which are two or three u below the compound system. These differences are due to the presence of small components of d, t, or ^{3}He emission. This effect was not observed for any of the other residue mass groups.

One method which has achieved some success in separating reaction products into direct products and fusion-evaporation products[2,8] is to compare the experimental energy (or velocity) spectra to statistical model predictions of the energy spectra. Each of the mass groups included in the fusion cross sections shown in Fig. 2 has an energy spectrum which is consistent with statistical model predictions. For example, one of the more interesting mass groups to study is the mass 13 group. Energy spectra for the $A=13$ mass group are shown in Fig. 7 for all four reactions. The potential mechanisms which could produce mass 13 products are many; in some reactions they could be produced as elastic scattering recoils, as the result of neutron transfers and as fusion-evaporation residues. From the similarity of the shapes of the four spectra in Fig. 8 it does not appear that the transfer reactions are a significant contribution to the observed yields. One can easily show by assuming Rutherford scattering for all c.m. angles that elastic scattering recoils are not important in the $\theta_{lab}=5-45$ range. Furthermore, the mass 13 energy distributions are peaked where expected in a fusion reaction.[2] In particular, energy distributions of $A=13$ products from the $^{6}Li + ^{13}C$ and $^{7}Li + ^{12}C$ collisions are the same within our experimental uncertainties. Furthermore, the residue energy where a particular mass

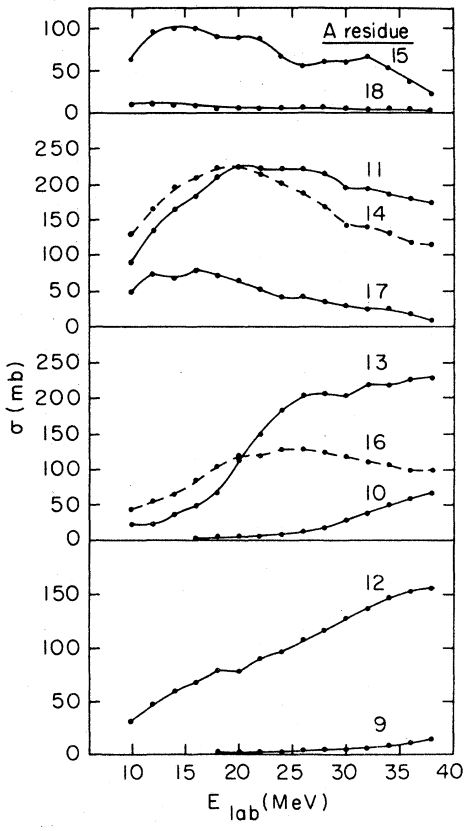

FIG. 6. Shown here are the excitation functions for the individual mass groups produced in the $^{7}Li + {}^{13}C$ reaction. The lines are drawn to help guide the eye.

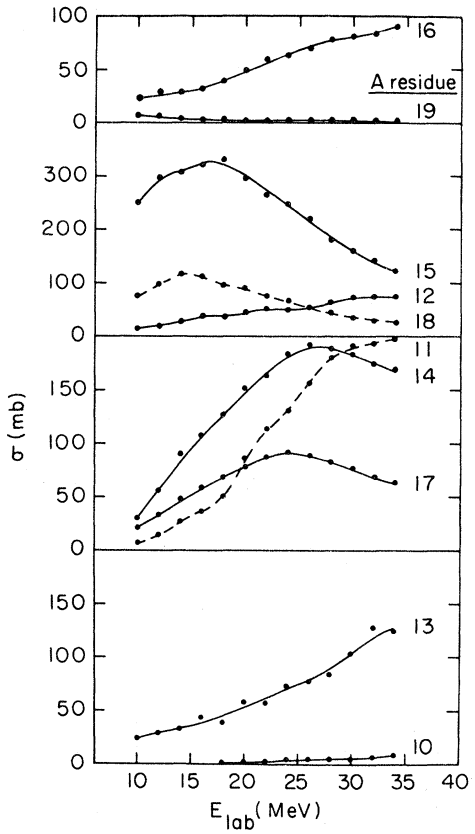

FIG. 7. Shown here are the excitation functions for the individual mass groups produced in the $^{7}Li + {}^{13}C$ reaction. The lines are drawn to help guide the eye.

yield peaks for the four reactions shows a systematic trend; the most probable residue energy decreases as the number of neutrons or protons which must be emitted to leave a particular residue increases. For example, the $^{6}Li + {}^{12}C$ reaction can produce mass 13 residues by evaporation of an alpha particle plus a proton or a neutron; the $^{6}Li + {}^{13}C$ reaction can produce a mass 13 residue by evaporation of an alpha particle plus 2 protons, 2 neutrons, or a neutron and a proton. The latter reaction requires emission of an extra light particle thus leaving less energy for the evaporation residue. This same trend is also observed in all four of the reactions. For example, in Fig. 1 the mass 18, 17, and 16 and the mass 14, 13, and 12 groups both show this trend. Thus these spectra confirm that the reaction products with mass 13 are produced predominantly by a fusion-evaporation reaction. A careful look at Fig. 1 shows some discrete peaks in the mass 6, 8, and 9 groups. A rough idea of the relative strengths of such direct processes and fusion can be obtained from Fig. 1. The yields for these discrete peaks were not included in the fusion cross sections. In this energy range the dominance of the fusion process is due in some sense to the selectivity of direct reactions for particular final states and grazing angular momentum values.

IV. DISCUSSION

Figure 3 shows the fusion excitation functions for all four reactions. All four excitation functions have similar shapes. The most surprising feature of these excitation functions is that the ^{6}Li induced reactions peak near $\sigma_{fus}=775$ mb, while the ^{7}Li induced reactions peak near 950 mb. This difference in the maximum fusion cross sections for the two projectiles indicates that the projectile plays an important role in determining the maximum fusion cross sections for these systems. Furthermore, we found that throughout the energy range the total

TABLE II. Maximum residue angles.

Reaction	Energy (MeV)	Residue (u)	θ_{max}[a]	θ_{max}[b]	θ_{max}^{expt}
		17	24		22
$^{6}Li + ^{12}C$	34	16	33	34	30
		15	30	38	35
		18	25		22
$^{6}Li + ^{13}C$	27.7	17	33	34	30
		16	38	48	>45
		18	22		20
$^{7}Li + ^{12}C$	30	17	27	29	29
		16	30	39	34
		19	23		21
$^{7}Li + ^{13}C$	28	18	30	31	30
		17	30	39	35

[a]Maximum kinematically allowed angle assuming only p and n are emitted.
[b]Maximum kinematically allowed angle assuming d, ^{3}He, or t emission.

TABLE III. Glas and Mosel parameters.

Reaction	r_B (fm)	V_B (MeV)	r_c (fm)	V_c (MeV)
$^{6}Li + ^{12}C$	1.38	4.30	1.06	−2.80
$^{6}Li + ^{13}C$	1.38	4.30	1.06	−2.80
$^{7}Li + ^{12}C$	1.54	4.30	1.13	−2.80
$^{7}Li + ^{13}C$	1.54	4.30	1.13	−2.80

fusion cross sections for these reactions were about a factor of 2 smaller than the total reaction cross section calculated using optical model parameters[9] which gave good fits to our measured elastic scattering angular distributions. Such large differences between the calculated total reaction cross sections and the measured fusion cross sections at all energies are not unique to these Li induced reactions. Similar observations were reported for the $^{9}Be + ^{28}Si$,[6] $^{11}B + ^{12}C$, and $^{10}B + ^{13}C$ (Ref. 10) reactions and it is of interest to perform similar studies of other reactions initiated by light projectiles to see how common such differences are.

Table III shows sets of Glas and Mosel parameters[4] used to fit the experimental fusion cross sections. Comparisons of the Glas and Mosel calculations and the experimental cross sections are shown in Fig. 9 for all four systems. The fits shown in Fig. 9 are quite good. As shown in Table III only the entrance channel barrier radius r_B needs to be changed markedly from reaction to reaction to obtain fits to all the data. This parameter needs to be changed only when the projectile changes, emphasizing that for these systems the differences in the maximum fusion cross sections are related to the entrance channel. What is surprising is that the radius parameter for the ^{7}Li induced reactions is larger than the radius parameter for the ^{6}Li induced reactions; in contrast, electron scattering results[11] indicate that ^{6}Li has a slightly larger root mean square (r.m.s.) radius than ^{7}Li. Thus the differences in the fusion excitation functions are not due to a simple size effect.

A model proposed by Kondo[12] to describe the maximum fusion cross sections is based on the idea that there is competition for entrance channel flux between fusion, inelastic, and direct reaction channels. Since ^{6}Li and ^{7}Li generally involve substantially different inelastic and direct channels, the fusion cross sections predicted by such a model could in principle be different. However, when we

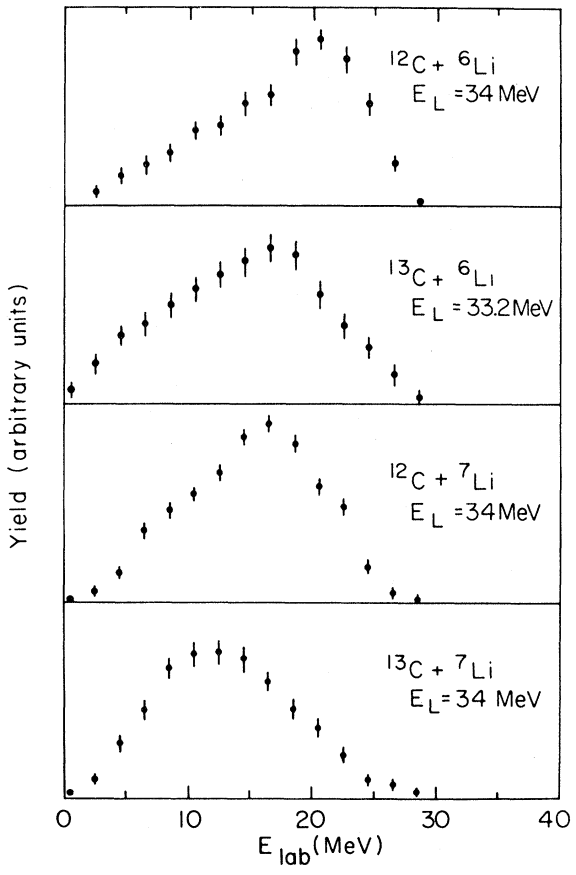

FIG. 8. This figure shows the energy distributions for the mass 13 evaporation residues for the reactions, lab energies, and angles given.

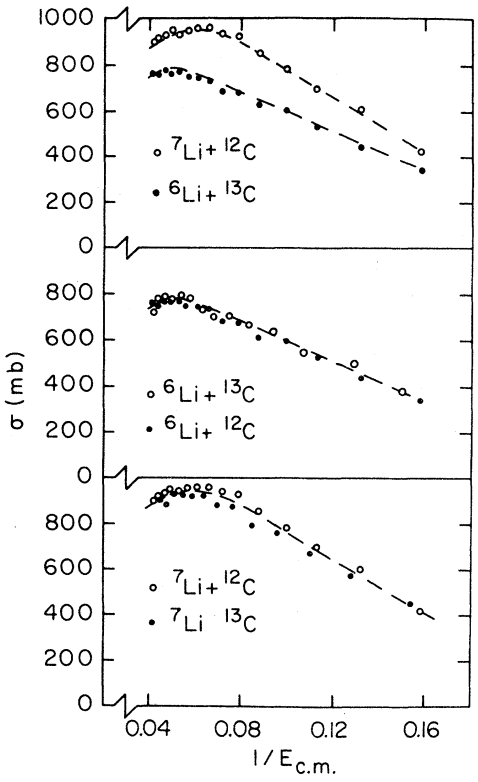

FIG. 9. Compared are the fusion cross sections versus $1/E_{\text{c.m.}}$ and the fusion cross sections calculated (dashed lines) using the Glas and Mosel parameters given in Table III. Only the barrier radius r_B varies from system to system.

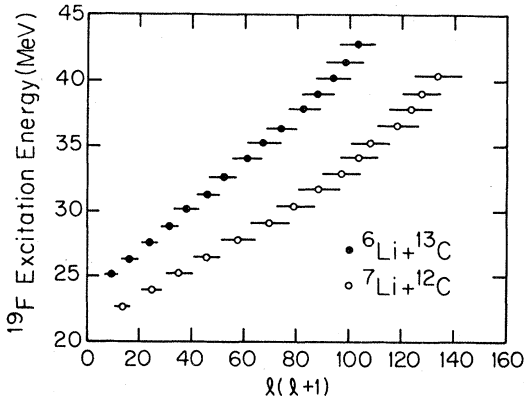

FIG. 10. Plotted are the critical angular momentum values [actually $l_c(l_c+1)$] extracted using the sharp-cutoff model from the $^6\text{Li} + ^{13}\text{C}$ and $^7\text{Li} + ^{12}\text{C}$ fusion cross sections versus the corresponding excitation energy for the compound nucleus formed by these entrance channels.

tried to use this model with transmission coefficients from calculations using standard optical model parameters for the $L+C$ entrance channels, the total reaction cross sections we obtained were roughly a factor of 2 larger than the fusion cross section throughout the energy range. The direct components calculated using Kondo's standard parameters are not nearly large enough to account for this difference.

The statistical yrast model of Lee *et al.*[3] attempts to explain the observed fusion cross sections by considering mechanisms that limit the angular momentum for these reactions. In the low energy region the contribution of each partial wave to fusion is determined by the transmission coefficient. At higher energies the fusion cross section is limited by the total angular momentum the compound nucleus can contain. Using this model the fusion cross sections for the $^6\text{Li} + ^{13}\text{C}$ and $^7\text{Li} + ^{12}\text{C}$ reactions should be the same in the high energy region when viewed on an excitation energy versus maximum angular momentum plot. As can be seen from Fig. 10 the data for the two entrance channels do not converge toward the same line at high excitation energies on such a plot. Much of our data for these two reactions lies in what Lee called region I, the low energy region. However, the high energy region as described in Ref. 3 should begin where the fusion cross section reaches a maximum, and so our data for both reactions extend well into the high energy region and the two E_x vs $l(l+1)$ curves should be converging if the Lee model is to describe this data.

V. CONCLUSIONS

The measurements of the fusion cross sections for $^6\text{Li} + ^{12}\text{C}$, $^6\text{Li} + ^{13}\text{C}$, $^7\text{Li} + ^{12}\text{C}$, and $^7\text{Li} + ^{13}\text{C}$ have produced several unexpected results. They show that the energy dependence of the fusion cross sections and the maximum fusion cross sections depend strongly on the projectile. Comparisons of the measured fusion cross sections with calculated total reaction cross sections indicate that the total reaction cross section is much larger than the fusion cross section. The ^7Li induced fusion reactions exhibit a significantly larger maximum fusion cross section, 950 ± 50 mb, than the ^6Li induced fusion reactions, which reach a maximum fusion cross section of 775 ± 40 mb. The energy spectra for the individual mass groups are qualitatively as expected for fusion evaporation reactions. There is evidence in the angular distributions that a small percentage of the evaporation residues are produced by d and t

or ^{3}He decays from the compound nucleus.

The differences in the fusion excitation functions are difficult to understand in terms of current ideas about the limitations of fusion reactions, yet they can be parametrized very well using the Glas and Mosel model by making the barrier radius parameter about 15% larger for the ^{7}Li induced reactions than for the ^{6}Li induced reactions.

---

*Present address: Department of Physics, Faculty of Science, University of Cairo, Giza, Egypt.

[1]D. G. Kovar, D. F. Geesaman, T. H. Braid, Y. Eisen, W. Henning, T. R. Ophel, M. Paul, K. E. Rehm, S. J. Sanders, P. Sperr, J. P. Schiffer, S. L. Tabor, S. Vigdor, B. Zeidman, and F. W. Prosser, Jr., Phys. Rev. C 20, 1305 (1979).

[2]J. Gomez del Campo, R. G. Stokstad, J. A. Biggerstaff, R. A. Dayras, A. H. Snell, and P. H. Stelson, Phys. Rev. C 19, 2170 (1979).

[3]S. M. Lee, T. Matsuse, and A. Arima, Phys. Rev. Lett. 45, 165 (1980).

[4]R. Bass, Phys. Rev. Lett. 39, 265 (1977).

[5]D. Glas and U. Mosel, Nucl. Phys. A237, 429 (1975).

[6]J. S. Eck, J. R. Leigh, T. R. Ophel, and P. D. Clark, Phys. Rev. C 21, 2352 (1980).

[7]A. D. Frawley, N. R. Fletcher, and L. C. Dennis, Phys. Rev. C 25, 860 (1982).

[8]P. A. DeYoung, J. J. Kolata, R. C. Luhn, R. E. Malmin, and S. N. Tripathi, Phys. Rev. C 24, 166 (1981).

[9]P. Schumacher, N. Ueta, H. H. Duhm, K.-I. Kubb, and W. G. Klages, Nucl. Phys. A212, 573 (1973).

[10]J. F. Mateja, A. D. Frawley, L. C. Dennis, K. Abdo, and K. W. Kemper, Phys. Rev. Lett. 47, 311 (1981).

[11]C. W. de Jager, H. de Vries, and C. de Vries, At. Data Nucl. Data Tables 14, 479 (1974).

[12]Y. Kondó, private communication.